Muhammad Baqar Hussain Shah, Qaisar Mansoor, Tariq Jan*, Zahid Farooq and Syed Zafar Ilyas

Synthesis of SnO_2 nanoparticles coated ZnO–g–C_3N_4 composite nanostructures with novel antibacterial activity

https://doi.org/10.1515/zna-2023-0032
Received February 13, 2023; accepted March 22, 2023;
published online April 10, 2023

Abstract: In this work, composite nanostructures (CNs) of SnO_2–ZnO–g–C_3N_4 have been prepared by a soft chemical method and investigated for their potential application in photocatalytic remediation of organics in water and antibacterial agents. Structural study revealed the presence of three phases related to hexagonal wurtzite phase of ZnO, tetragonal phase of SnO_2 and monoclinic phase of g–C_3N_4 having nanocrystalline nature which confirms the formation of CNs. Formation of nanoscale morphology along with elemental composition of the CNs have been validated through scanning electron microscopy (SEM) coupled with energy dispersive X-ray (EDX) spectroscopy. The presence of only A_{1g} mode of SnO_2 in Raman spectrum of ternary CNs suggested that SnO_2 nanoparticles have been coated on the surfaces of ZnO and g–C_3N_4 which is also evident from SEM results. SnO_2–ZnO–g–C_3N_4 CNs have shown much higher photocatalytic degradation efficiency and produced 7 mm greater zone of inhibition (ZOI) against Gram-positive *S. Aureus* bacteria as compared to pure ZnO which is quite significant result when compared to previously reported results for SnO_2–ZnO CNs. These synthesized CNs may have potential uses in healthcare technology and treatment of organics in water.

Keywords: antibacterial activity; composite nanostructures; g–C_3N_4; SnO_2; ZnO

***Corresponding author: Tariq Jan**, Department of Physics, Allama Iqbal Open University, Islamabad, Pakistan, E-mail: tariq.jan@aiou.edu.pk
Muhammad Baqar Hussain Shah and Syed Zafar Ilyas, Department of Physics, Allama Iqbal Open University, Islamabad, Pakistan
Qaisar Mansoor, Institute of Biomedical and Genetic Engineering (IBGE), Islamabad, Pakistan
Zahid Farooq, Department of Physics, University of Education (Lahore), Faisalabad Campus, Faisalabad, Pakistan

1 Introduction

The development of resistant bacterial strains due abnormal use of antibiotics has led to alarming stubborn infectious diseases worldwide [1]. The resistant nature of bacterial strains to currently available conventional antibiotics is growing day by day which demands development of novel nonconventional antibiotics. In this regard, scientists are looking up a solution in inorganic nanomaterials. Nanomaterials have unique physiochemical properties along with unique mechanisms of action against bacterial strains thus reducing chances of development of resistance in bacterial strains against nanomaterials. Among various classes of nanomaterials, metal oxide nanomaterials are believed to be the best choice for antibacterial applications due to low cost, easy processing, biocompatibility, and antibacterial activities [2]. To date, many metal oxide nanomaterials are explored for this purpose such as ZnO, CuO, TiO_2, SnO_2, Ag_2O, etc. [3–7]. Among them, ZnO outclass other nanomaterials because of greater biocompatibility, wide band gap of 3.37 eV, essential excitonic binding energy of 60 meV, biologically and chemically inert nature, comparatively greater antibacterial activity, and cost effectiveness [3, 8]. However, the antibacterial activity of ZnO nanostructures is still below par for practical application as antibiotic due to low reactive oxygen species (ROS) generation because of fast electron hole pair recombination and large agglomeration in solution due to surface effects [9]. These drawbacks of ZnO nanostructures may be overcome by making its nanocomposites with other metal oxide having suitable band positions which will reduce electron-hole pair recombination rate. SnO_2 may be the best choice for this purpose because of its higher electron mobility which will lead to faster transport of photogenerated electrons and moreover, conduction band (CB) of SnO_2 is more positive than ZnO which means its CB may act as electron sink for photogenerated electrons in ZnO [10]. Thus SnO_2–ZnO composite nanostructures (CNs) will have lower electron–hole pair recombination rate. This is why several research groups worldwide have explored these CNs for photocatalytic and antibacterial applications. Xingkun Liang et al.; reported enhanced

antibacterial activity of SnO_2–ZnO composite attributed to increased ROS production [11]. While S. K. Evstropiev et al.; associated the improved antibacterial activity of ZnO–SnO_2 coatings to microstructural variations caused by addition of SnO_2 to ZnO [12]. Monica Pandey et al.; have concluded in their study that mixed oxide CNs shows better antibacterial activities as compared pristine ZnO linked to higher electronic interactions, but the zone of inhibition (ZOI) reported for SnO_2–ZnO CNs is found to be below 10 mm against various bacterial strains [13]. This suggests that although SnO_2–ZnO CNs demonstrates higher antibacterial activity, but it still needs to be improved. This can be achieved by combining SnO_2–ZnO CNs with g–C_3N_4 to make ternary CNs. Recently these ternary CNs have been reported to have enhanced photocatalytic activity due to enhanced speed of electron transfer, lower electron–hole pair recombination rate, and high specific surface area [14]. As all these three phenomena play crucial role in antibacterial activity, hence it is expected that this ternary CNs will have enhanced antibacterial activity.

2 Materials and methods

2.1 Synthesis of g–C_3N_4

g–C_3N_4 was prepared by heating urea in muffle furnace at 550 °C for 5 h at heating rate of 10 °C/min. After cooling it down to room temperature, solid g–C_3N_4 was obtained.

2.2 Synthesis of ZnO–g–C_3N_4

For synthesis of ZnO–g–C_3N_4 CNs, 0.5 g of g–C_3N_4 was suspended in distilled water and zinc nitrate and hexamethylenetetramine (HTMA) were added to make 0.05 M solution. The pH value of solution was raised to 8 by adding 1 M NaOH solution drop by drop. Afterwards, the solution was kept on stirring at 80 °C for 2 h. After 2 h, the solution was cooled down to room temperature and centrifuged to get the precipitates. The precipitates were washed three times with distilled water and dried in electric oven at 120 °C for 5 h. The dried precipitates were then annealed at 500 °C for 5 h in furnace to get highly crystalline ZnO–g–C_3N_4 CNs.

2.3 Synthesis of SnO_2–ZnO–g–C_3N_4 ternary CNs

SnO_2–ZnO–g–C_3N_4 ternary CNs were prepared by suspending one g of ZnO–g–C_3N_4 CNs in 100 mL distilled water and tin chloride and HTMA were added to make 0.05 M solution. Afterwards, a similar procedure was adopted as being used for synthesis of ZnO–g–C_3N_4 CNs. these synthesized CNs were characterized using X-ray diffraction (XRD), SEM, EDX, and Raman spectroscopy techniques.

2.4 Photocatalytic degradation of methylene blue (MB) dye

The photocatalytic activity of SnO_2–ZnO–g–C_3N_4 ternary CNs was measured under irradiation of natural sunlight. 15 mg of nanoparticles were added to 50 mL solution of MB dye and kept for 30 min in dark under constant stirring. After 30 min, the suspensions were illuminated with direct sunlight. After each interval of 20 min, 2 mL of suspension was collected and centrifuged for 3 min. Then absorption spectrum was recorded using UV-visible absorption spectrometer.

2.5 Antibacterial activity

Antibacterial activity of the prepared CNs was evaluated using disc diffusion method. A single colony of Gram-positive *Staphylococcus aureus (S. Aureus)* bacteria was cultured by lawn formation method. Then colloidal suspensions of the prepared CNs, ZnO nanoparticles having concentrations of 50 μg/mL were applied to agar petri plates. One disc was placed in culture without presence of nanostructures and named as control. Finally, these agar plates were incubated at 37 °C for 24 h and zone of inhibition (ZOI) were measured in millimeters (mm).

3 Results and discussions

3.1 Structural and morphological properties

Structural properties of the prepared ZnO and SnO_2–ZnO–g–C_3N_4 ternary CNs were investigated through XRD using Cu k_α X-rays having wavelength of 1.54 Å in two theta range of 20–70°. The diffraction pattern of ZnO exhibited peaks originated from reflections from planes of hexagonal wurtzite structure of ZnO. SnO_2–ZnO–g–C_3N_4 ternary CNs diffraction pattern revealed the presence of peaks related to hexagonal wurtzite structure of ZnO, tetragonal phase of SnO_2 and monoclinic phase of g–C_3N_4 as shown in Figure 1 [15–17]. Positions of some peaks of hexagonal ZnO and tetragonal SnO_2 appear at same two theta values therefore, there is strong possibility of merging of peaks related to both ZnO and SnO_2 in two theta range of 30–40°. The presence of peaks related to ZnO, SnO_2 and g–C_3N_4 confirm the formation of ternary CNs. The intensities of diffraction peaks of ZnO have decreased significantly in CNs which indicated the decrement in crystalline quality of ZnO. Moreover, absence of any impurities related peaks demonstrates the phase purity of the synthesized samples. Average crystallite size of ZnO was calculated using Scherer formula given by;

$$D = \frac{k\lambda}{\beta \cos \theta}$$

where D is average crystallite size, k is shape constant having value of 0.89, λ is wavelength of X-rays being used,

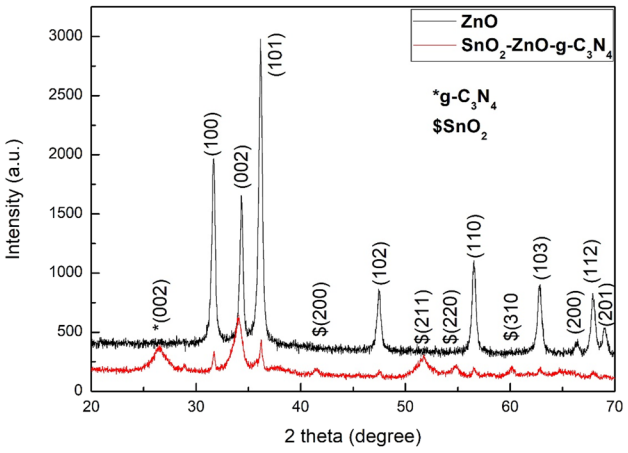

Figure 1: XRD patterns of the prepared samples.

β is full width at half maximum in radians, and θ is the diffraction angle in degrees. The average crystallite size for pristine ZnO sample has been calculated to be 23 nm which is increased to 45 nm for CNs. This agrees well with the previously reported trend that addition of SnO_2 leads to larger crystallite size of ZnO [18].

In addition to XRD analysis, SEM coupled with EDX was used for morphology and elemental composition of the SnO_2–ZnO–g–C_3N_4 ternary CNs. Figure 2 shows the SEM image of CNs revealing the presence of tiny spherical nanoparticles of SnO_2 are being coated on the surfaces of g–C_3N_4 sheets and ZnO nanoparticles having average particle size of 51 nm. The average particle size obtained from SEM is very close to the average crystallite size calculated from XRD results. The EDX spectrum shows the existence of peaks related to Zn, Sn, C, and O which supports the claim of ternary CNs as shown in Figure 3. The presence of peaks related Au is due to Au coating of the sample. Hence, XRD, SEM, and EDX analysis confirm the formation of phase pure SnO_2–ZnO–g–C_3N_4 ternary CNs having high degree of chemical purity.

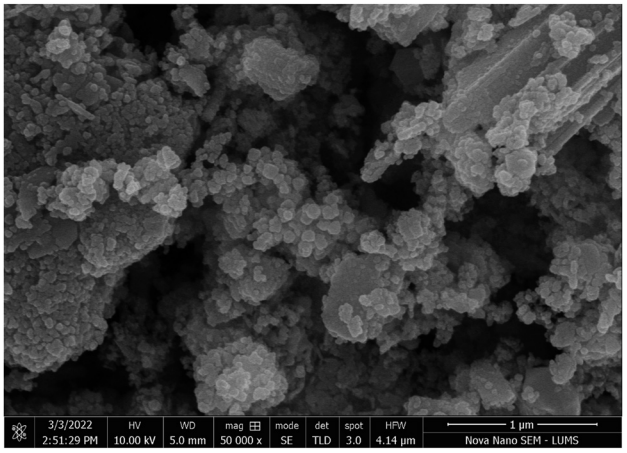

Figure 2: SEM image of SnO_2–ZnO–g–C_3N_4 CNs.

3.2 Raman study

The structural and vibrational properties of the prepared nanomaterials were studied using Raman spectroscopy technique. Figure 4 depicts the Raman spectrum of pure ZnO and SnO_2–ZnO–g–C_3N_4 ternary CNs. Number of peaks in lower wavenumber region can be seen from the Raman spectrum of pure ZnO positioned at 334.43 cm^{-1}, 436.7 cm^{-1}, 522.8 cm^{-1}, and 584.33 cm^{-1} which may be assigned to the vibrations from $E_{2H} - E_{2L}$, E_{2H}, $E_{2H} + E_{2L}$, and E_1^{LO} vibrational modes of hexagonal wurtzite structure of ZnO [19]. The presence of E_{2H} mode associated with oxygen vibration is the indication of formation of typical wurtzite lattice of ZnO and its high intensity demonstrate that the prepared ZnO sample has greater crystallinity. Moreover, the presence of E_1^{LO} is mostly associated with formation of defects in ZnO lattice [19, 20]. In higher wavenumber region, only peak can be seen positioned at 1133 cm^{-1} which arises from the contribution of $2A_1^{LO}$ and $2E_1^{LO}$ modes at Γ point of the Brillouin zone [21]. When we look at Raman spectrum of CNs, all the peaks associated with vibrational modes of hexagonal ZnO disappeared and only one broad peak is present at wavenumber of ranging from 638 to 687 cm^{-1}. It is previously reported that peak positioned at 638 cm^{-1} is assigned to A_{1g} mode of SnO_2 [22]. While usually Raman forbidden band appears at 693 cm^{-1} for nanoparticles of SnO_2 due to their high surface area [22]. The appearance of this broad peak may be due to the combination of these two bands. The absence of ZnO vibrational modes in CNs may be justified due to the fact that SnO_2 is coated on the surface of ZnO which leads to suppression of its modes. Previously, similar results were reported for carbon coated zinc ferrite nanoparticles [23].

3.3 Photocatalytic and antibacterial activity

The photocatalytic degradation ability of the synthesized ternary CNs was evaluated towards MB dye in aqueous solution under natural sunlight. Figure 5 shows the absorption curves of MB dye recorded at different times of exposure to sunlight in the presence of SnO_2–ZnO–g–C_3N_4 ternary CNs. It is evident from this figure; absorption intensity gradually decreases with increase in exposure time. This decrease in intensity of absorption peak exhibits the degradation of MB dye in the presence of ternary CNs. SnO_2–ZnO–g–C_3N_4

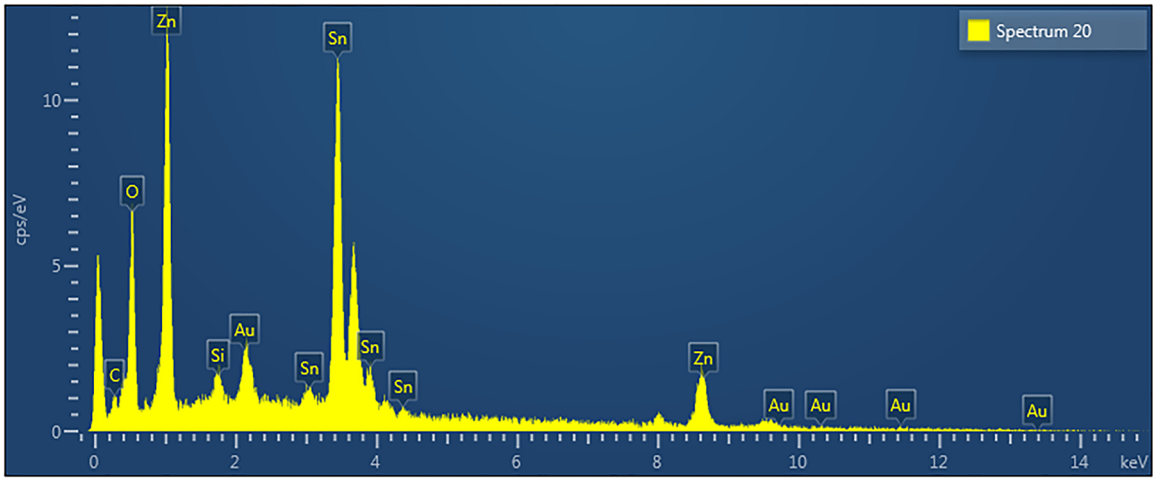

Figure 3: EDX spectrum of CNs.

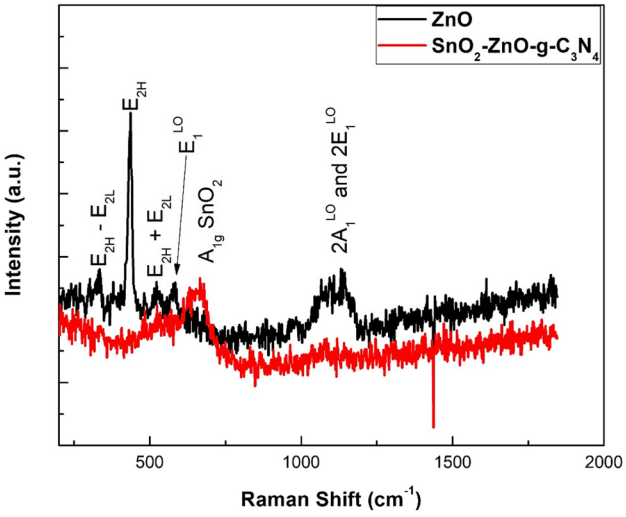

Figure 4: Room temperature Raman spectra of ZnO and SnO_2–ZnO–g–C_3N_4 CNs.

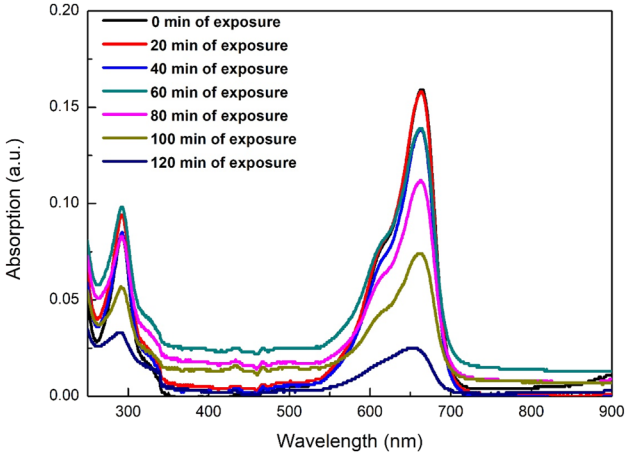

Figure 5: Evolution of MB dye absorption spectra in the presence of CNs.

ternary CNs. The degradation efficiency of the synthesized ternary CNs was evaluated by formula.

$$D\% = \frac{C_0 - C}{C_0} \times 100$$

where $D\%$ is the degradation efficiency, C_0 is initial concentration after equilibrium, and C is concentration at any given time. It is evident from Figure 6 that SnO_2–ZnO–g–C_3N_4 ternary CNs have better efficiency of 84.5 % than that of pure ZnO (51 %) under sunlight irradiation for 120 min. The conduction band (CB) potential of g–C_3N_4 is more negative than CB potential of both ZnO and SnO_2 which makes it feasible that electrons will transfer from g–C_3N_4 to oxide semiconductors [14]. This will reduce electron–hole pair recombination rate thereby leading to enhanced photocatalytic degradation of MB dye. The electrons will interact with dissolved oxygen and form superoxide anion radicals while holes will interact with water and create hydroxyl radicals on the surface of ternary CNs. These produced radicals will degrade MB dye by oxidizing its molecules due to their strong oxidative nature.

Finally, antibacterial activity of the synthesized SnO_2–ZnO–g–C_3N_4 ternary CNs was evaluated against Gram-positive *S. Aureus* bacteria. The prepared CNs have produced ZOI of 23 mm which is 7 mm greater than that created ZnO (16 mm) as shown in Figure 7(b) and (c), respectively. Moreover, the observed value of ZOI for SnO_2–ZnO–g–C_3N_4 ternary CNs is much greater than those previously reported for mixed oxides of ZnO and SnO_2 [12, 24, 25]. Figure 7(a) is a control sample without presence

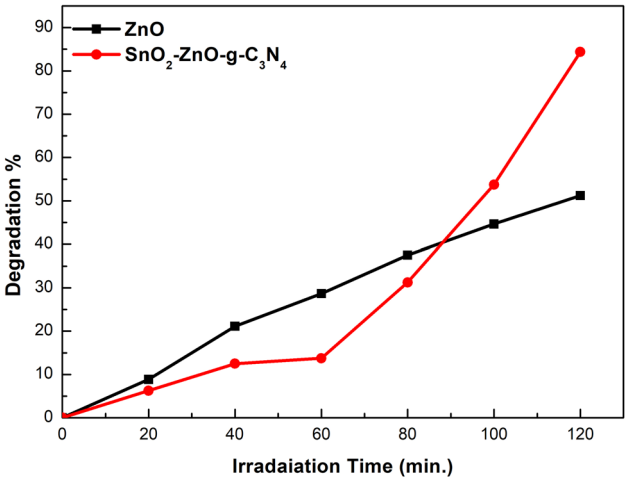

Figure 6: Photocatalytic degradation efficiency of ZnO nanoparticles and SnO_2–ZnO–g–C_3N_4 ternary CNs.

of nanoparticles. The synthesized SnO_2–ZnO–g–C_3N_4 ternary CNs has remarkably enhanced antibacterial activity as compared to ZnO. This enhanced antibacterial activity of the synthesized ternary CNs may be linked to various factors. It is plausible to assume that the ternary CNs may have strong electronic interaction in cooperative manner leading to rupturing or distortion of bilayer membrane of bacterial cells more effectively than ZnO [13]. As it is previously reported that SnO_2 addition to ZnO leads stronger interaction with positively charged biomolecules at the cell surface of Gram-positive bacteria [26]. The other plausible reason for enhanced antibacterial activity of ternary CNs may be associated with enhanced ROS production which is also evident from photocatalytic experiments. These generated ROS restrain the biological processes in bacteria and causing their death. Hence, the remarkably enhanced antibacterial activity of SnO_2–ZnO–g–C_3N_4 ternary CNs may be attributed to strong electrostatic interactions between CNs and positively charged surface of bacteria and enhanced ROS production.

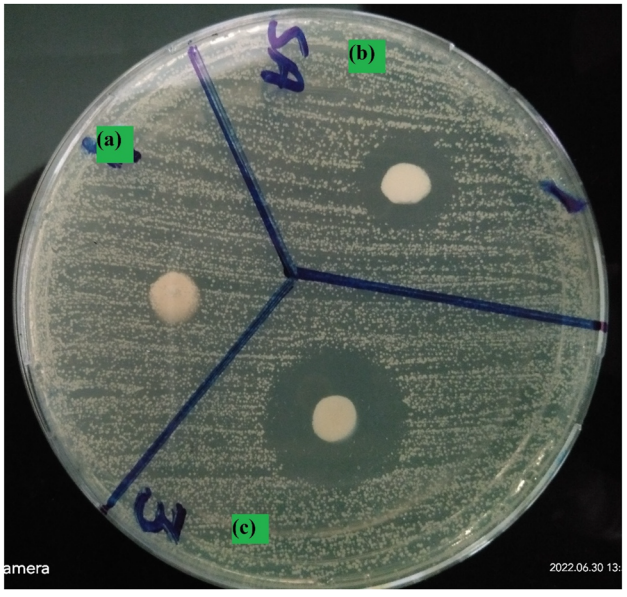

Figure 7: ZOI results obtained for (a) control, (b) ZnO nanoparticles, and (c) SnO_2–ZnO–g–C_3N_4 ternary CNs.

4 Conclusions

In conclusion, ternary CNs of SnO_2–ZnO–g–C_3N_4 were successfully prepared via a simple wet chemical method. The structural, morphological, vibrational, photocatalytic, and antibacterial characteristics were comprehensively investigated by XRD, SEM, Raman, UV-visible absorption spectroscopy and agar disc diffusion method. The prepared ternary CNs have shown enhanced photocatalytic degradation efficiency towards MB dye compared to pure ZnO which was attributed to reduced electron–hole pair recombination rate due to better separation. Moreover, SnO_2–ZnO–g–C_3N_4 ternary CNs have produced ZOI of 23 mm which is larger than previously reported for SnO_2–ZnO CNs. Hence, these CNs may have potential application for degradation of organics in water and antibacterial agents.

Author contributions: All the authors have accepted responsibility for the entire content of this submitted manuscript and approved submission.

Research funding: Corresponding author acknowledges the financial support by AIOU, Islamabad, Pakistan.

Conflict of interest statement: The authors report no conflict of interest in this work and data will be provided on reasonable request.

References

[1] A. Raghunath and E. Perumal, "Metal oxide nanoparticles as antimicrobial agents: a promise for the future," *Int. J. Antimicrob. Agents*, vol. 49, no. 2, pp. 137–152, 2017.

[2] Y. Li, W. Zhang, J. Niu, and Y. Chen, "Mechanism of photogenerated reactive oxygen species and correlation with the antibacterial properties of engineered metal-oxide nanoparticles," *ACS Nano*, vol. 6, no. 6, pp. 5164–5173, 2012.

[3] B. Mohapatra, S. Choudhary, S. Mohapatra, and S. Sharma, "Facile preparation and antibacterial activity of zinc oxide nanobullets," *Mater. Today Commun.*, vol. 34, p. 105083, 2023.

[4] T. Jan, S. Azmat, Q. Mansoor, et al., "Structural, Raman, optical and novel antibacterial characteristics of Al doped CuO nanostructures," *Mater. Res. Express*, vol. 6, no. 10, pp. 0—10, 2019.
[5] A. J. jafari and M. Moslemzadeh, "The effect of TiO2 nanoparticles on bacterial growth: the effect of particle size and their structure—a systematic review," *Int. J. Environ. Health Res.*, pp. 1—11, 2022, https://doi.org/10.1080/09603123.2022.2163990.
[6] N. Y. Elamin, T. Indumathi, and E. R. Kumar, "Evaluation of physicochemical and biological properties of SnO2 and Fe doped SnO2 nanoparticles," *Ceram. Int.*, vol. 49, no. 2, pp. 2388—2393, 2023.
[7] A. H. Mohammadi, A. Sobhani-Nasab, M. Nejati, et al, "Preparation and characterization of CuO, Ag2O and ZnO nanoparticles and investigation of their antibacterial and anticancer properties on HCT-116 and C26 cells," *Inorg. Chem. Commun.*, vol. 149, p. 110404, 2023.
[8] M. Malekkiani, A. Heshmati Jannat Magham, F. Ravari, and M. Dadmehr, "Facile fabrication of ternary MWCNTs/ZnO/Chitosan nanocomposite for enhanced photocatalytic degradation of methylene blue and antibacterial activity," *Sci. Rep.*, vol. 12, no. 1, pp. 1—22, 2022.
[9] M. Li, Z. Chen, Y. Sun, et al., "Preparation and antibacterial activity of graphene oxide/cuprous oxide/zinc oxide nanocomposite," *Mater. Res. Express*, vol. 8, no. 12, pp. 1—10, 2021.
[10] Y. Yu, B. Yao, B. Cao, and W. Ma, "Morphology-controlled fabrication of SnO2/ZnO nanocomposites with enhanced photocatalytic performance," *Photochem. Photobiol.*, vol. 95, no. 5, pp. 1131—1141, 2019.
[11] X. Liang, R. Dai, H. Ma, X. Tang, and B. Zhang, "Synergistic antibacterial properties of ZnO—SnO2 composite under both light and dark conditions," *Ceram. Int.*, vol. 48, no. 21, pp. 32089—32103, 2022.
[12] S. K. Evstropiev, A. Karavaeva, M. Petrova, et al., "Antibacterial effect of nanostructured ZnO-SnO2 coatings: the role of microstructure," *Mater. Today Commun.*, vol. 21, p. 100628, 2019.
[13] M. Pandey, M. Singh, K. Wasnik, et al., "Targeted and enhanced antimicrobial inhibition of mesoporous ZnO-Ag2O/Ag, ZnO-CuO, and ZnO-SnO2Composite nanoparticles," *ACS Omega*, vol. 6, no. 47, pp. 31615—31631, 2021.
[14] S. V. P. Vattikuti, P. A. K. Reddy, J. Shim, and C. Byon, "Visible-Light-driven photocatalytic activity of SnO2-ZnO quantum dots anchored on g-C3N4 nanosheets for photocatalytic pollutant degradation and H2 production," *ACS Omega*, vol. 3, no. 7, pp. 7587—7602, 2018.
[15] S. A. Ansari, M. M. Khan, S. Kalathil, A. Nisar, J. Lee, and M. H. Cho, "Oxygen vacancy induced band gap narrowing of ZnO nanostructures by an electrochemically active biofilm," *Nanoscale*, vol. 5, no. 19, pp. 9238—9246, 2013.
[16] D. Hu, B. Han, S. Deng, et al., "Novel mixed phase SnO2 nanorods assembled with SnO2 nanocrystals for enhancing gas-sensing performance toward isopropanol gas," *J. Phys. Chem. C*, vol. 118, no. 18, pp. 9832—9840, 2014.
[17] S. V. P. Vattikuti and C. Byon, "Hydrothermally synthesized ternary heterostructured MoS2/Al2O3/g-C3N4 photocatalyst," *Mater. Res. Bull.*, vol. 96, pp. 233—245, 2017.
[18] M. T. Uddin, M. E. Hoque, and M. Chandra Bhoumick, "Facile one-pot synthesis of heterostructure SnO2/ZnO photocatalyst for enhanced photocatalytic degradation of organic dye," *RSC Adv.*, vol. 10, no. 40, pp. 23554—23565, 2020.
[19] H. K. Yadav, K. Sreenivas, V. Gupta, and R. S. Katiyar, "Structural studies and Raman spectroscopy of forbidden zone boundary phonons in Ni-doped ZnO ceramics," *J. Raman Spectrosc.*, vol. 40, no. 4, pp. 381—386, 2009.
[20] T. Jan, J. Iqbal, M. Ismail, and A. Mahmood, "Synthesis of highly efficient antibacterial agent Ag doped ZnO nanorods: structural, Raman and optical properties," *J. Appl. Phys.*, vol. 115, no. 15, p. 154308, 2014.
[21] R. Cusco, E. Alarcón-Lladó, J. Ibáñez, et al., "Temperature dependence of Raman scattering in ZnO," *Phys. Rev. B*, vol. 75, no. 16, p. 165202, 2007.
[22] I. M. Costa, Y. N. Colmenares, P. S. Pizani, E. R. Leite, and A. J. Chiquito, "Sb doping of VLS synthesized SnO2 nanowires probed by Raman and XPS spectroscopy," *Chem. Phys. Lett.*, vol. 695, pp. 125—130, 2018.
[23] L. Cabo-Fernandez, F. Mueller, S. Passerini, and L. J. Hardwick, "In situ Raman spectroscopy of carbon-coated ZnFe2O4 anode material in Li-ion batteries — investigation of SEI growth," *Chem. Commun.*, vol. 52, no. 20, pp. 3970—3973, 2016.
[24] S. K. Evstropiev, A. V. Karavaeva, N. V. Nikonorov, V. N. Vasilyev, and A. S. Saratovskii, "Structural engineering of ZnO—SnO2—Ag (AgCl) nanocomposites for the medical applications," *J. Inorg. Organomet. Polym. Mater.*, vol. 311, no. 11, pp. 4373—4383, 2022.
[25] N. Arasavalli, D. R. Alli, B. K. Babu, G. Ravichandra, and K. S. Mokshagni, "ZnO: SnO2 nanocomposite efficacy for gas sensing and microbial applications," *Indian J. Biochem. Biophys.*, vol. 59, no. 5, pp. 586—594, 2022.
[26] A. Chávez-Calderón, F. Paraguay-Delgado, E. Orrantia-Borunda, and A. Luna-Velasco, "Size effect of SnO2 nanoparticles on bacteria toxicity and their membrane damage," *Chemosphere*, vol. 165, pp. 33—40, 2016.